

## All-Ceramic Microfibrous Solar Steam Generator: TiN Plasmonic Nanoparticle-Loaded Transparent Microfibers

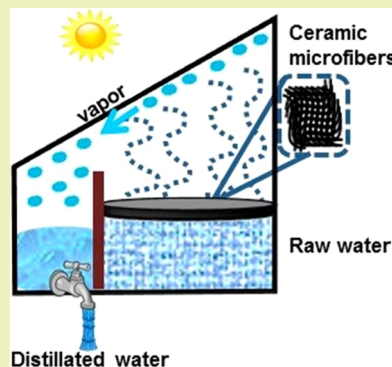
Manpreet Kaur,<sup>†,‡,§</sup> Satoshi Ishii,<sup>\*,†,§</sup> Satish Laxman Shinde,<sup>†,§</sup> and Tadaaki Nagao<sup>\*,†,‡,§</sup>

<sup>†</sup>International Center for Materials Nanoarchitectonics (WPI-MANA), National Institute for Materials Science (NIMS), 1-1 Namiki, Tsukuba, Ibaraki 305-0044, Japan

<sup>‡</sup>Department of Condensed Matter Physics, Hokkaido University, 5 Chome Kita 8 Jonishi, Kita Ward, Sapporo, Hokkaido 060-0810, Japan

### Supporting Information

**ABSTRACT:** A portable and reusable solar water distillation structure based on low cost ceramic materials is developed. The structure is made of ceramic fiber wool (CW) and titanium nitride nanoparticles (TiN NPs) that are chemically immobilized to the CW. When sunlight illuminates the structure, the TiN NPs absorb sunlight while unnecessary heating of the remaining water is suppressed by the CW. The CW effectively supply water by capillary force such that the TiN NPs are always kept close to the water surface. It yields a solar thermal conversion efficiency of more than 80% at  $100 \text{ mW cm}^{-2}$  that is much more efficient than the conventional systems. Our structures can be used as eco-friendly and efficient solar water distillator.



**KEYWORDS:** Nanoparticle, Titanium nitride, Surface modification, Composite material

### INTRODUCTION

Solar heat is a simple yet efficient way of utilizing solar energy. The most common type of solar thermal collector utilizes black absorbers such as black colored panels or tubes to absorb sunlight and heat the fluid, which is typically water for domestic use.<sup>1–3</sup> In contrast, attempts to directly heat liquids for solar heating have been made since the early 1970s;<sup>4,5</sup> in early studies, black ink was mixed into the liquid. Nanoparticles (NPs) can be used as sunlight absorbers in the liquid to form a “nanofluid”.<sup>6–8</sup> In a nanofluid, the NPs absorb sunlight and directly heat the liquid (i.e., photothermal conversion)<sup>9,10</sup> without losing heat to the outside environment. Various NPs have been explored as sunlight-absorbing NPs, such as metals,<sup>11,12</sup> alloys,<sup>13–15</sup> ceramics,<sup>16</sup> semiconductors,<sup>17,18</sup> and carbon-based materials.<sup>19,20</sup> In recent years, plasmonic NPs have attracted considerable attention because they can function as subwavelength antennas to efficiently collect light at their plasmon resonances. Owing to the strong field localization and subsequent local heating at the plasmon resonances, plasmonic NPs not only are efficient materials for heating water but also can vaporize water rapidly.<sup>21</sup> Among the studies on plasmonic photothermal effects, gold NPs have been predominantly used because of their strong plasmonic resonances and chemical stability.<sup>22–25</sup> Recently, conductive ceramic titanium nitride (TiN) NPs have been considered as alternative materials to gold owing to the strong plasmon resonances. The adequate losses of TiN cause the absorption spectrum to be broad, but the plasmon resonance of the TiN NPs remains strong, which

is favorable for the absorption of sunlight in the wavelength range of ultraviolet (UV) to near-infrared (NIR).<sup>26,27</sup> TiN NPs have been used for solar photothermal studies and have outperformed gold and carbon NPs at identical concentrations.<sup>28–30</sup> In addition, TiN is far more cost-effective than gold and is a chemically stable ceramic, making TiN NPs promising candidates for mass-produced sunlight absorbers.

Though the dispersion of sunlight-absorbing NPs in water and other liquids has been studied,<sup>30</sup> attaching them to a host makes them easy to handle and reuse. In this regard, mesoporous alumina, which has a large surface area, is useful for facilitating capillary force,<sup>31–33</sup> and has been used with plasmonic NPs for solar water distillation. Other porous structures such as paper and polyurethane are as well investigated.<sup>34–36</sup> Taking advantage of capillary force is vital for constantly conveying the water to the forefront of the vaporization. Transparent ceramic microfiber wools (CW) can function as a different type of host material, also having a large surface area and narrow adjacent spacings for capillary forces. In addition, CW are generally cheaper and more easily mass-produced than porous alumina. However, CW have attracted little attention in the context of solar heat generators thus far.

Herein, we propose the use of transparent CW in combination with broadband TiN NPs to form a highly

Received: June 26, 2017

Revised: August 26, 2017

Published: September 14, 2017

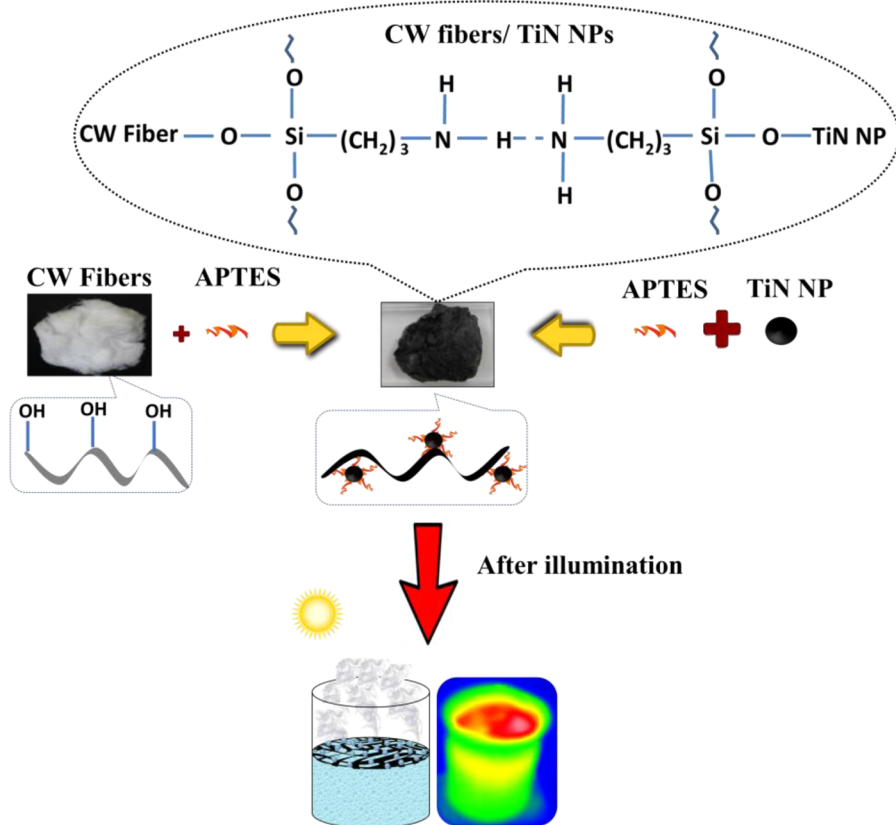


**Figure 1.** Schematic represents the fabrication process of TCW structure with possible interactions scheme between CW fibers and TiN NPs. OH group modified CW as well as TiN NPs are functionalized with coupling agent APTES separately. TiN NPs immobilized onto CW (TCW) shows steam generation after illumination.

efficient all-ceramic hybrid solar absorber (hereinafter referred to as TCW). We chemically immobilized TiN NPs on CW to form an eco-friendly ceramic sunlight absorber to heat and vaporize water. Because the TiN NPs were firmly attached to the CW, they did not dissipate in the water, making them easy to collect and remove from the water container. This is an important feature that makes the TiN NP-based sunlight absorber reusable and easy to carry. Measurements for evaluating the vaporization of water by sunlight revealed that the TCWs had a higher efficiency than the TiN NPs dispersed in water. The excellent energy-conversion efficiency and reusability of the present materials will pave the way for practical solar-heating applications of ceramic nanostructures.

The TiN NPs used in the study were synthesized via the thermal plasma method,<sup>37</sup> and their average size was ~40 nm. The CW (ISOWOOL Blankets 1260; Isolite Insulating Products Co. Ltd.) were composed of microfibers of transparent oxides ( $\text{SiO}_2$  53%,  $\text{Al}_2\text{O}_3$  46%,  $\text{TiO}_2$  0.5%) having a mean fiber diameter of approximately 3.2  $\mu\text{m}$ . To attach the TiN NPs to the CW, (3-aminopropyl)triethoxysilane (APTES, Merck Schuchardt OHG) was used. The TiN NP concentration was varied from 50 to 400 mg per 1000 mg of CW in water. TiN NPs of 50, 100, 200, 300, and 400 mg were added to 10 mL of pure water containing 1000 mg of CW to form TCWs, which were labeled as 0.5T, 1T, 2T, 3T, and 4T, respectively, for sample identification. Figure 1 shows schematics and photographs of the sample preparation. Hydrophobic CW were modified into hydrophilic ones after obtaining the OH group from sodium hydroxide (additional details are provided in the Experimental Section). Hydroxyl

(OH) groups on the CW surface helped to form hydrogen bonds between the water and the fibers. In addition to the hydrogen bonding sites, the interspacing of the fibers can induce a capillary force, resulting in the sucking up of water at the air–water interface. We functionalized TiN NPs by using coupling agents (APTES) to promote the interfacial adhesion between the TiN NPs and the CW, as shown in Figure 1. The TiN NPs were agglomerated and closely packed on the CW, which play an important role in broadband sunlight absorption. The functionalization of the CW and TiN NPs were confirmed by Fourier transform infrared spectroscopy (FTIR) (Nicolet iS50R, Thermo Scientific) as presented in Figure S1 in the Supporting Information.

Figure 2a plots the UV–visible (UV–vis) absorbance spectra (V-570, JASCO) measured before and after the TiN NPs were functionalized with APTES. The absorption spectrum of TiN NPs dispersed in water shows a broad LSPR peak in the visible–NIR region. The APTES-functionalized TiN NPs showed similar but broader peak. The broadening is due to the aggregation of the TiN NPs, which was confirmed by a particle analyzer (ELS-Z-2000, Otsuka Electronics) (137 nm for pristine TiN NPs and 801 nm for APTES-functionalized TiN NPs). The absorbance of the TiN NPs immobilized ceramic wool (TCW) is calculated from its reflectance spectra and shown in Figure 2b. The broad absorbance peak of the TCW in the visible–NIR region is indicative of LSPR peak of the TiN NPs. When we compare the absorption spectra of the TCW to that of the unfunctionalized TiN NPs dispersed in water (TS) (Figure 2a.), we observed red shift and further broadening in the

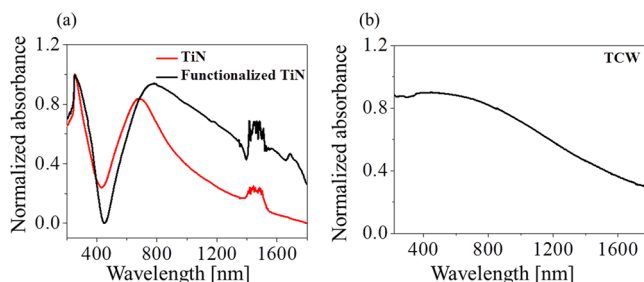


**Figure 2.** (a) Normalized UV–vis absorbance spectra of the TiN NPs and functionalized TiN NPs. (b) Absorbance spectra of TiN NPs immobilized onto CW (TCW). The small peak around 1400 nm for TiN and functionalized TiN is due to water absorption that is not fully normalized.

absorbance spectra. This is most likely due to the aggregation of the TiN NPs at the TCW.

Figure 3a,b shows scanning electron microscopy (SEM, SU8000, Hitachi) images of the CW and TiN NPs, indicating

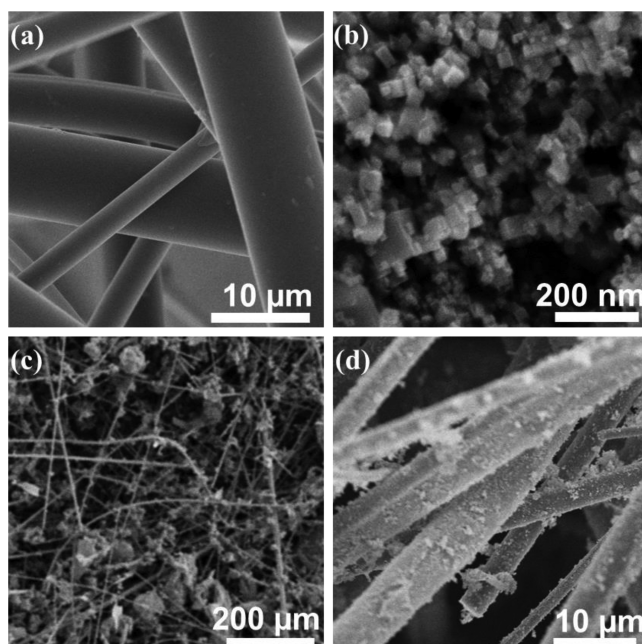


**Figure 3.** FE-SEM images of (a) CW (b) TiN NPs (c, d) TCW (3T). Image d is the high magnification image of image c.

their cubic and fibrous structures, respectively. The TEM image of the TiN NPs is shown in Figure S2. Figure 3c,d shows images taken after the TiN NPs were immobilized on the CW as TCW. The SEM images of the other TCWs are shown in Figure S3 in the Supporting Information. The SEM images clearly show that the TiN NPs were agglomerated and attached along the surface of the CW.

The crystallinity of the samples was characterized via X-ray diffraction (XRD, RINT 2000, Rigaku). All the peaks are indexed to TiN (JCPDS card No. 064909). The XRD patterns plotted in Figure 4a reveal face-centered cubic crystalline TiN NPs. The TiN NPs exhibit peaks that are assigned to (111), (200), (220), (311), and (222) diffraction at angles of 36.70°, 42.63°, 61.87°, 74.145°, and 78.04°, respectively. The diffraction pattern of the CW exhibited a broad feature corresponding to an amorphous structure (Figure 4b).

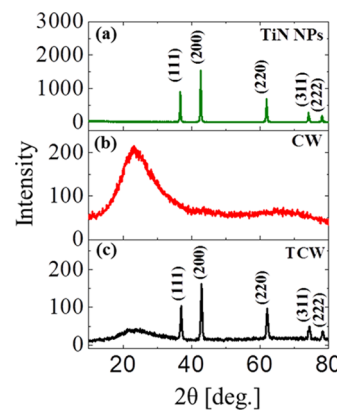


**Figure 4.** X-ray diffraction patterns of (a) TiN NPs (b) CW (c) TiN NPs immobilized onto CW.

However, after the immobilization of the TiN NPs, the XRD pattern of the TCW also exhibited sharp peaks corresponding to TiN NPs, as shown in Figure 4c, indicating that the crystallinity of the TiN NPs was not affected by the fabrication of the TCW.

Another important characteristic of the TCWs is their optical reflectance, or in turn optical absorptance. Using an integrating sphere, reflectance measurements were performed. The sample was placed on a white circular tile at the sample port of a UV–vis spectrophotometer (V-570, JASCO). The relative defused reflectance was measured with the reflectance of the CW as a reference. The reflectance spectra are shown in Figure 5. The

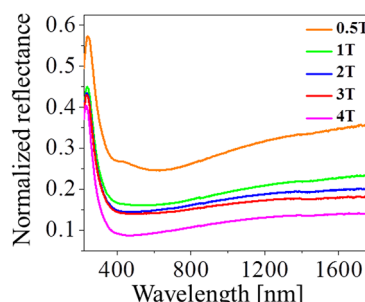


**Figure 5.** UV–vis reflectance spectra of TCW with different concentration of TiN NPs.

reflectance decreased as the TiN NP concentration loaded onto the CW increased, indicating that the amount of TiN NPs attached to the CW depended on the original concentration of the TiN colloid suspension. Because the transmittance was zero for all the samples, the monotonic decrease of the reflectance indicates that the absorption increased with the TiN NP concentration loaded onto the CW.

The energy conversion from sunlight to heat and the vaporization of water were tested using a solar simulator (XES-40S1, San-Ei Electric), where the AM 1.5 spectrum was guaranteed. An electric balance (AUW220D, Shimadzu) and a type-K thermocouple were used to measure the weight and temperature changes, respectively, during the artificial sunlight illumination.

During the measurements, 50 mL of pure water, as well as TCW, was added to a 50 mL Pyrex beaker, which was placed into a hollow container made of polystyrene foam for thermal isolation. The top of the container was open, allowing vapor to exit. The room temperature and relative humidity of the lab

environment were 20–21 °C and 44–51%, respectively. Except for the irradiance of the solar simulator, all the conditions were kept the same for the measurements. The schematic and photo of the experimental setup is shown in Figure S4.

Figure 6a,b summarizes the time-dependent temperature increase and weight changes of the TCW with different

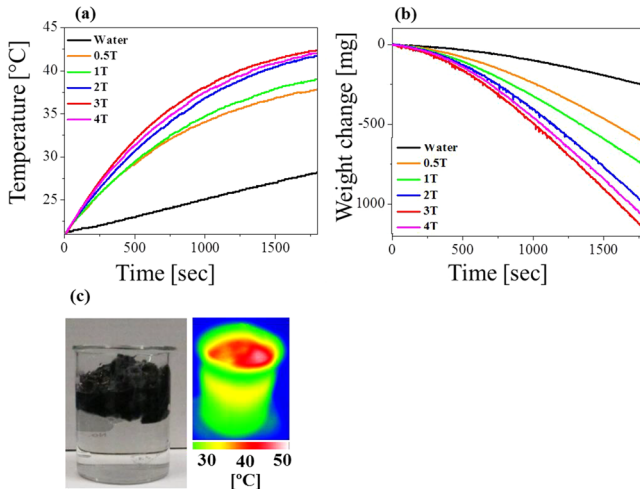


**Figure 6.** (a) Temperature change and (b) weight change of TCW due to vapor generation, having different concentration of TiN NPs upon  $100 \text{ mW cm}^{-2}$  illumination power for 1800 s (c) Photo of floating TCW without illumination and IR camera image during experiment with temperature scale (pure CW is used below TCW to make it float).

concentrations of TiN NPs under  $100 \text{ mW cm}^{-2}$  illumination. A photo of the TCW and an infrared-camera image taken under the artificial sunlight illumination are shown in Figure 6c, indicating the heat concentration in the TCW. The temperature-increase and vapor-generation rates increased in proportion to the NP concentration loaded onto the CW. However, concentrations higher than 3T did not significantly increase the vaporization or the weight change. In fact, slight reductions in the temperature and weight change were observed when the TCW concentration increased above 3T. We postulate that water heating and evaporation rates are basically proportional to the TiN NP concentration up to certain concentration, and there is an optimal concentration to maximize the water heating and evaporation rates. Thus, optimizing the concentration of TiN NPs in TCW is important for maximizing the solar-heating performance.

Comparative studies on the vaporization and temperature changes were performed using TCW (3T), TiN NPs dissolved in water (300 mg TiN NPs into 50 mL, labeled as TS), and CW. The amount of water for all three samples was fixed to 50 mL, which differs from our previous work.<sup>30</sup> The results are shown in Figure 7a,b, indicating the high efficiency of the TCW compared with the TS and CW. The temperature increased from 21 to 42.37 °C, and the weight loss was 1160 mg after 1800 s. An additional comparison was performed under focused  $500 \text{ mW cm}^{-2}$  sunlight from the solar simulator, as shown in Figure 8. Again, there was again a significant performance difference between the TiN NPs immobilized on CW and the same amount of the TiN NPs dispersed in 50 mL of water (TS). Though the TCW temperature swiftly increased to 50 °C within 600 s, in the case of TS, the temperature increased moderately to 43 °C after 1800 s. The evaporated weight of

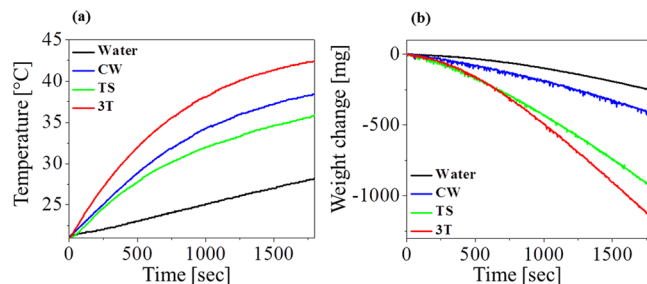


**Figure 7.** (a) Temperature change and (b) weight change of pure water, CW, TiN NP, and TCWs (3T) at the irradiance of  $100 \text{ mW cm}^{-2}$  for 1800 s.

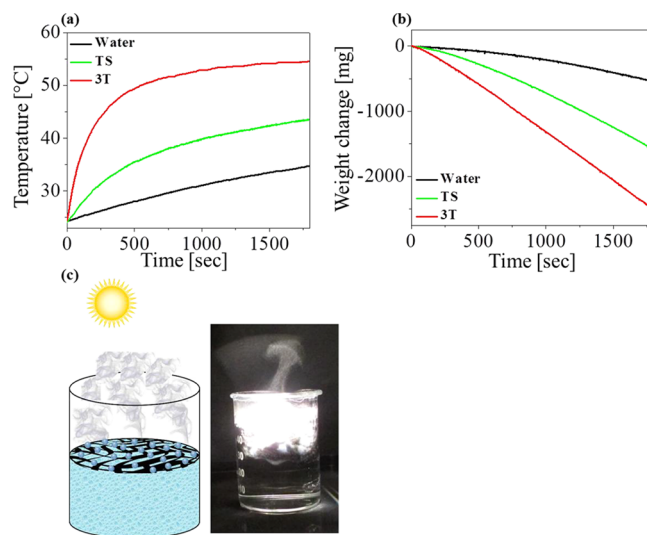


**Figure 8.** (a) Temperature change and (b) weight change of pure water, TiN NPs dispersed into water (TS) and TCW (3T) at the irradiance of  $500 \text{ mW cm}^{-2}$  for 1800 s. The photo in panel c was taken under the solar irradiance of  $500 \text{ mW cm}^{-2}$ . TCW floating on water (pure CW is used below TCW to make it float successfully at air–water interface).

water for the TCW was greater than that for TS by 933 mg. After 1800 s, the maximum temperature reached 54 °C, and the weight changes caused by the TCW reached 2,520 mg. Figure 8c illustrates the steam generation obtained by using a TCW under concentrated solar illumination of  $500 \text{ mW cm}^{-2}$  at room temperature (also see Video in the Supporting Information). Vapor generation at room temperature is a distinct indication of heat localization around the TiN NPs.<sup>30</sup>

As shown in Figures 7 and 8, TCW had a higher performance than TS. The major factors making the TCW an efficient sunlight absorber were its large surface area and high particle density. The specific surface areas measured via the Brunauer–Emmett–Teller method (Quantachrome, Autosorb-iQ) for the TiN NPs and TCW (3T) were  $463.79$  and  $2068.98 \text{ cm}^2 \text{ mg}^{-1}$ , respectively. The particle densities of the TS and TCW (3T) were  $1.73 \times 10^{13}$  and  $2 \times 10^{16} \text{ cm}^{-3}$ , respectively. These results show that the surface area and particle density of the TCW were several times larger than those of the TS. The larger surface area due to the high particle density resulted in a larger temperature increase and greater steam generation for the TCW. Nevertheless, as shown in Figure 6, care must be taken not to overload TiN NPs for TCWs.

Finally, the conversion efficiency was calculated by using the weight loss and temperature increase as output values and the illumination intensity as an input value. At 100 mW cm<sup>-2</sup> irradiance, the conversion efficiency of the TCW (3T) was >80%, and 44% of the illuminated light was consumed for water evaporation. With this efficiency, 8.8 L of distilled water can be produced from a 1 m<sup>2</sup> TCW surface in 1 h at 500 mW cm<sup>-2</sup>, according to an extrapolation of our results. The evaporation speed of TCW is faster than that of the other systems.<sup>31,33,34,38</sup> In addition, durability of the TCW were evaluated as shown in Figures S5 in the Supporting Information and the TCW was proved to be usable for multiple times. We postulate that this study represents a practical approach for the design and fabrication of reusable, low-cost, light, and highly efficient materials for solar steam generation and solar-heating systems.

In conclusion, we developed a cost-effective composite structure by combining TiN NPs and CW and demonstrated its use as a highly efficient, reusable, and portable sunlight absorber. The broadband absorption of TiN NPs is advantageous for applications involving steam generation via sunlight and nanoscale heat localization. Under the experimental conditions, the steam-generation efficiency of TCW was higher than that of TiN NPs dispersed in water and pure CW dispersed in water. The effective capillary force generated by the fibrous structure of the composite, as well as the high light concentration and photothermal conversion of the immobilized TiN NP, allowed excellent solar steam generation. Our study on the ceramic composite contributes to the efficient use of solar energy and the development of simple and low-cost devices for clean water generation.

## EXPERIMENTAL SECTION

To combine TiN NPs with CW, (3-aminopropyl)triethoxysilane (APTES) was used. The TiN NPs were refluxed with APTES solution in ethanol: H<sub>2</sub>O = 8:2 at 80 °C for 30 min. The extra amount of APTES and ethanol was separated and removed after centrifuging the TiN suspension at 9000 rpm. The amine-terminated TiN NPs were extracted and redispersed in water. The CW were cleaned with sodium hydroxide solution and immersed into APTES solution to functionalize. And then they were dipped into modified TiN NPs dispersed solution for 1 h. Afterward, the TiN-loaded CW were rinsed with water thoroughly and dried at 80 °C for overnight.

## ASSOCIATED CONTENT

### Supporting Information

The Supporting Information is available free of charge on the ACS Publications website at DOI: [10.1021/acssuschemeng.7b02089](https://doi.org/10.1021/acssuschemeng.7b02089).

Steam generation obtained by using the TCW under concentrated solar illumination of 500 mW cm<sup>-2</sup> at room temperature ([AVI](#))

FTIR spectra of the TiN NPs, CW, and TCW; TEM image of the TiN NPs; SEM images of the TCWs; schematic of the experimental setup; reusability tests ([PDF](#))

## AUTHOR INFORMATION

### Corresponding Authors

\*S. Ishii. E-mail: [sishii@nims.go.jp](mailto:sishii@nims.go.jp).

\*T. Nagao. E-mail: [NAGAO.Tadaaki@nims.go.jp](mailto:NAGAO.Tadaaki@nims.go.jp).

### ORCID

Manpreet Kaur: [0000-0003-3511-7797](https://orcid.org/0000-0003-3511-7797)

Satoshi Ishii: [0000-0003-0731-8428](https://orcid.org/0000-0003-0731-8428)

Satish Laxman Shinde: [0000-0002-0353-3705](https://orcid.org/0000-0002-0353-3705)

Tadaaki Nagao: [0000-0002-6746-2686](https://orcid.org/0000-0002-6746-2686)

### Notes

The authors declare no competing financial interest.

## ACKNOWLEDGMENTS

This work is partially supported by the JSPS KAKENHI (JP15K17447, JP16H06364, JP16K17496, 17H04801), CREST “Phase Interface Science for Highly Efficient Energy Utilization” (JPMJCR13C3) by the Japan Science and Technology Agency and the Japan Prize Foundation.

## REFERENCES

- (1) Burke, A.; Etter, D.; Hudgens, C.; Wiedenheft, C.; Wittenberg, L. Thermal and photochemical studies of solar energy absorbers dissolved in heat transfer fluids. *Sol. Energy Mater.* **1982**, *6* (4), 481–490.
- (2) Sorour, M. Developments in solar water heaters. *Energy Convers. Manage.* **1985**, *25* (3), 365–372.
- (3) Hordy, N.; Rabilloud, D.; Meunier, J.-L.; Coulombe, S. High temperature and long-term stability of carbon nanotube nanofluids for direct absorption solar thermal collectors. *Sol. Energy* **2014**, *105*, 82–90.
- (4) Minardi, J. E.; Chuang, H. N. Performance of a “black” liquid flat-plate solar collector. *Sol. Energy* **1975**, *17* (3), 179–183.
- (5) Huang, B.; Nieh, S. Measurements of the total transmittance of the solar radiation through an absorbing black liquid water. *Lett. Heat Mass Transfer* **1979**, *6* (1), 57–60.
- (6) Otanicar, T. P.; Phelan, P. E.; Prasher, R. S.; Rosengarten, G.; Taylor, R. A. Nanofluid-based direct absorption solar collector. *J. Renewable Sustainable Energy* **2010**, *2* (3), 033102.
- (7) Mahian, O.; Kianifar, A.; Kalogirou, S. A.; Pop, I.; Wongwises, S. A review of the applications of nanofluids in solar energy. *Int. J. Heat Mass Transfer* **2013**, *57* (2), 582–594.
- (8) Moghadam, A. J.; Farzane-Gord, M.; Sajadi, M.; Hoseyn-Zadeh, M. Effects of CuO/water nanofluid on the efficiency of a flat-plate solar collector. *Exp. Therm. Fluid Sci.* **2014**, *58*, 9–14.
- (9) Link, S.; El-Sayed, M. A. Shape and size dependence of radiative, non-radiative and photothermal properties of gold nanocrystals. *Int. Rev. Phys. Chem.* **2000**, *19* (3), 409–453.
- (10) Chen, H.; Shao, L.; Ming, T.; Sun, Z.; Zhao, C.; Yang, B.; Wang, J. Understanding the photothermal conversion efficiency of gold nanocrystals. *Small* **2010**, *6* (20), 2272–2280.
- (11) Govorov, A. O.; Richardson, H. H. Generating heat with metal nanoparticles. *Nano Today* **2007**, *2* (1), 30–38.
- (12) Lukianova-Hleb, E. Y.; Lapotko, D. O. Influence of transient environmental photothermal effects on optical scattering by gold nanoparticles. *Nano Lett.* **2009**, *9* (5), 2160–2166.
- (13) Fabbri, L.; Fournier, D.; Pottier, L.; Esposito, L. Analysis of local heat transfer properties of tape-cast AlN ceramics using photothermal reflectance microscopy. *J. Mater. Sci.* **1996**, *31* (20), 5429–5436.
- (14) Tian, Q.; Jiang, F.; Zou, R.; Liu, Q.; Chen, Z.; Zhu, M.; Yang, S.; Wang, J.; Wang, J.; Hu, J. Hydrophilic Cu9S8 nanocrystals: A photothermal agent with a 25.7% heat conversion efficiency for photothermal ablation of cancer cells in vivo. *ACS Nano* **2011**, *5* (12), 9761–9771.
- (15) He, R.; Wang, Y.-C.; Wang, X.; Wang, Z.; Liu, G.; Zhou, W.; Wen, L.; Li, Q.; Wang, X.; Chen, X., et al. Facile synthesis of pentacle gold–copper alloy nanocrystals and their plasmonic and catalytic properties. *Nat. Commun.* **2014**, *5*, DOI: [10.1038/ncomms5327](https://doi.org/10.1038/ncomms5327).
- (16) Wang, N.; Yao, B.; Chan, Y.; Zhang, X. Enhanced photothermal effect in Si nanowires. *Nano Lett.* **2003**, *3* (4), 475–477.
- (17) Hessel, C. M.; Pattani, V. P.; Rasch, M.; Panthani, M. G.; Koo, B.; Tunnell, J. W.; Korgel, B. A. Copper selenide nanocrystals for photothermal therapy. *Nano Lett.* **2011**, *11* (6), 2560–2566.

- (18) Mandelis, A. Laser infrared photothermal radiometry of semiconductors: principles and applications to solid state electronics. *Solid-State Electron.* **1998**, *42* (1), 1–15.
- (19) Neumann, O.; Urban, A. S.; Day, J.; Lal, S.; Nordlander, P.; Halas, N. J. Solar vapor generation enabled by nanoparticles. *ACS Nano* **2013**, *7* (1), 42–49.
- (20) Han, D.; Meng, Z.; Wu, D.; Zhang, C.; Zhu, H. Thermal properties of carbon black aqueous nanofluids for solar absorption. *Nanoscale Res. Lett.* **2011**, *6* (1), 457.
- (21) Wang, Z.; Liu, Y.; Tao, P.; Shen, Q.; Yi, N.; Zhang, F.; Liu, Q.; Song, C.; Zhang, D.; Shang, W.; et al. Bio-Inspired Evaporation Through Plasmonic Film of Nanoparticles at the Air–Water Interface. *Small* **2014**, *10* (16), 3234–3239.
- (22) Cortie, M. B.; Xu, X.; Chowdhury, H.; Zareie, H.; Smith, G. Plasmonic heating of gold nanoparticles and its exploitation. In *Smart Materials, Nano-, and Micro-Smart Systems II*, Society of Photo-Optical Instrumentation Engineers: Bellingham, WA, 2004; Vol. 5649, pp 565–573.
- (23) Jiang, K.; Smith, D. A.; Pinchuk, A. Size-dependent Photothermal conversion efficiencies of plasmonically heated gold nanoparticles. *J. Phys. Chem. C* **2013**, *117* (51), 27073–27080.
- (24) Huang, X.; Jain, P. K.; El-Sayed, I. H.; El-Sayed, M. A. Plasmonic photothermal therapy (PPTT) using gold nanoparticles. *Lasers Med. Sci.* **2008**, *23* (3), 217–228.
- (25) Chen, X.; Zhu, H. Y.; Zhao, J. C.; Zheng, Z. F.; Gao, X. P. Visible-light-driven oxidation of organic contaminants in air with gold nanoparticle catalysts on oxide supports. *Angew. Chem.* **2008**, *120* (29), 5433–5436.
- (26) Li, W.; Guler, U.; Kinsey, N.; Naik, G. V.; Boltasseva, A.; Guan, J.; Shalaev, V. M.; Kildishev, A. V. Refractory plasmonics with titanium nitride: broadband metamaterial absorber. *Adv. Mater.* **2014**, *26* (47), 7959–7965.
- (27) Guler, U.; Suslov, S.; Kildishev, A. V.; Boltasseva, A.; Shalaev, V. M. Colloidal Plasmonic Titanium Nitride Nanoparticles: Properties and Applications. *Nanophotonics* **2015**, *4* (1), 269–276.
- (28) Guler, U.; Naik, G. V.; Boltasseva, A.; Shalaev, V. M.; Kildishev, A. V. Performance analysis of nitride alternative plasmonic materials for localized surface plasmon applications. *Appl. Phys. B: Lasers Opt.* **2012**, *107* (2), 285–291.
- (29) Guler, U.; Ndukaife, J. C.; Naik, G. V.; Nnanna, A. A.; Kildishev, A. V.; Shalaev, V. M.; Boltasseva, A. Local heating with lithographically fabricated plasmonic titanium nitride nanoparticles. *Nano Lett.* **2013**, *13* (12), 6078–6083.
- (30) Ishii, S.; Sugavaneshwar, R. P.; Nagao, T. Titanium Nitride Nanoparticles as Plasmonic Solar Heat Transducers. *J. Phys. Chem. C* **2016**, *120* (4), 2343–2348.
- (31) Zhou, L.; Tan, Y.; Ji, D.; Zhu, B.; Zhang, P.; Xu, J.; Gan, Q.; Yu, Z.; Zhu, J. Self-assembly of highly efficient, broadband plasmonic absorbers for solar steam generation. *Sci. Adv.* **2016**, *2* (4), No. e1501227.
- (32) Liu, Y.; Lou, J.; Ni, M.; Song, C.; Wu, J.; Dasgupta, N. P.; Tao, P.; Shang, W.; Deng, T. Bioinspired bifunctional membrane for efficient clean water generation. *ACS Appl. Mater. Interfaces* **2016**, *8* (1), 772–779.
- (33) Zhou, L.; Tan, Y.; Wang, J.; Xu, W.; Yuan, Y.; Cai, W.; Zhu, S.; Zhu, J. 3D self-assembly of aluminium nanoparticles for plasmon-enhanced solar desalination. *Nat. Photonics* **2016**, *10*, 393.
- (34) Liu, Y.; Yu, S.; Feng, R.; Bernard, A.; Liu, Y.; Zhang, Y.; Duan, H.; Shang, W.; Tao, P.; Song, C.; et al. A Bioinspired, Reusable, Paper-Based System for High-Performance Large-Scale Evaporation. *Adv. Mater.* **2015**, *27* (17), 2768–2774.
- (35) Liu, Y.; Wang, X.; Wu, H. High-performance wastewater treatment based on reusable functional photo-absorbers. *Chem. Eng. J.* **2017**, *309*, 787–794.
- (36) Wang, G.; Fu, Y.; Guo, A.; Mei, T.; Wang, J.; Li, J.; Wang, X. Reduced graphene oxide-polyurethane nanocomposite foams as a reusable photo-receiver for efficient solar steam generation. *Chem. Mater.* **2017**, *29*, 5629.
- (37) Nakamura, K. Synthesis of nanoparticles by thermal plasma processing and its applications. *Eurozoru Kenkyu* **2014**, *29* (2), 98–103.
- (38) Ito, Y.; Tanabe, Y.; Han, J.; Fujita, T.; Tanigaki, K.; Chen, M. Multifunctional Porous Graphene for High-Efficiency Steam Generation by Heat Localization. *Adv. Mater.* **2015**, *27* (29), 4302–4307.